Appl. Phys. B 49, 39–47 (1989)

Applied Physics B Photophysics and Laser Chemistry

Characterization of an Ethylene Free Jet

N. Dam and J. Reuss

Fysisch Laboratorium, Catholic University, Toernooiveld, NL-6525 ED Nijmegen, The Netherlands

Received 4 January 1989/Accepted 15 February 1989

Abstract. The rotational population distribution in a free molecular jet of ethylene, C_2H_4, is found to be thermal over a range of distances below the nozzle ($z/d = 0.5$–13.2, nozzle diameter $d = 0.50$ mm). Results for on-axis rotational temperature, number density and flow velocity are presented. The average number of gas-kinetic collisions experienced by any molecule in travelling some distance along the jet axis is calculated.

PACS: 34.50.Ez, 47.55.Cy

Two main experimental techniques in studying (gas phase) molecular spectroscopy and collision dynamics employ, roughly speaking, the gas cell and the molecular beam, both with their own advantages and drawbacks. The low number density and temperature obtained in a molecular beam as well as the possible beam collimation, reduce Doppler and pressure broadening and also the number of spectral lines observed, whereas spectra obtained from a gas cell, the lower limit on temperature usually being imposed by the freezing point of the gas, contain lines originating from many rotational (and vibrational) states, each with Doppler broadened width. From the point of view of an experimentalist on molecular collision dynamics, a gas cell may have more serious drawbacks. The molecules in a cell have a random thermal velocity (zero on average), their number density can often not be made as small as desired and wall effects (including adsorption and desorption) are hard to exclude. Molecules in a molecular beam, on the other hand, have a flow velocity which is sharply defined in both magnitude and direction. This allows to discriminate the beam molecules against the background gas. Furthermore the beam molecules can be directed to a collision target. The number density in the beam is so low that collisions within the beam can usually be neglected.

Intermediate between a gas cell and a molecular beam is a free molecular jet. It is formed by expanding a high pressure gas through a pinhole (the nozzle) into a low pressure chamber and in fact comprises the first stage in the formation of a molecular beam. Within a distance of a few nozzle diameters, the flow velocity of the molecules in the jet and its internal temperature have reached their final values, while number density and translational temperature keep on decreasing with increasing distance from the nozzle. The highly inhomogeneous region close to the nozzle makes for an interesting environment in studying molecular collisions but, in a sense, is less suitable for doing spectroscopy, because the diverging gas flow causes a large Doppler broadening of spectral lines, in spite of the relatively low temperatures in the jet.

In this contribution, the characterization of the jet properties, for the specific case of a free jet of ethylene, C_2H_4, will be discussed. One of the attractive features of ethylene is that it has strong absorption bands in the regions of the CO_2 laser (ν_7 at 948 cm^{-1}) and the Color Center Laser (CCL) (ν_9 at 3105 cm^{-1}; see Fig. 1). The rovibrational spectra in these regions are quite well understood. Near coincidences of ν_7 transitions with CO_2 laser lines have been listed by Herlemont et al. [1]. Spectroscopic data concerning the ν_9 band can be found in the survey by Pine [2].

The molecule ethylene, C_2H_4, is nearly a prolate symmetric top. Its rotational energy levels are designated by (J, K_{-1}, K_{+1}), in which K_{+1} can take on the values of $J-K_{-1}$ and $J-K_{-1}+1$ (but $0 \leqq K_{+1} \leqq J$). Because the C_2H_4 molecule is only nearly symmetric, levels with different K_{+1} values are not quite degenerate. For low J values the splitting is small, except for $K_{-1}=1$. Since the molecule possesses two pairs of

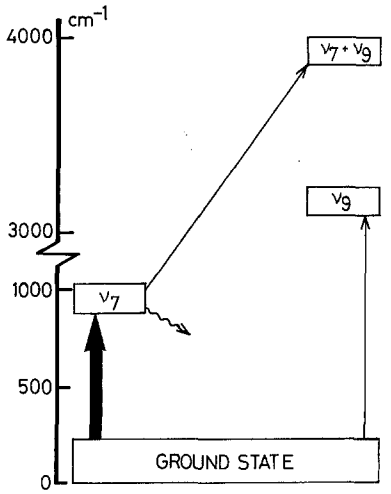

Fig. 1. Part of the vibrational energy level scheme of ethylene. The CO_2 laser acts between ground state and ν_7 (fat arrow). The probe laser can be tuned over the ν_9 fundamental band and its associated hot bands (thin arrows). Collisional relaxation from the ν_7 is indicated by a wavy arrow

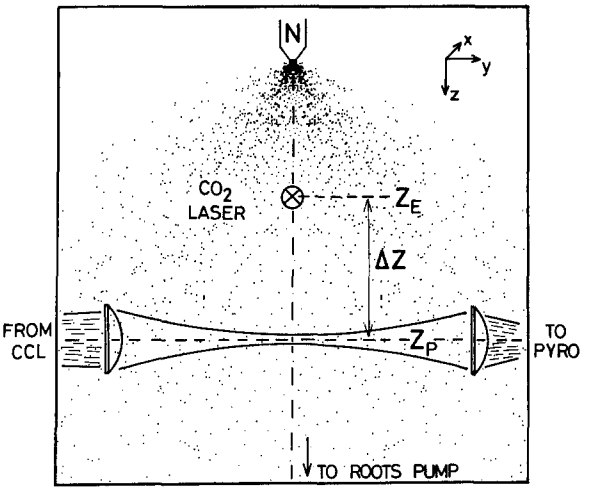

Fig. 2. Schematic view of the jet configuration. The nozzle N is made of stainless steel, with a drilled hole of 0.50 mm diameter. The CO_2 laser (going into the plane of the figure) is focussed on the jet axis at an (adjustable) distance z_E below the nozzle. At a distance z_P below the nozzle (also adjustable), the CCL beam is focussed on the jet axis. Afterwards, the beam is collected by another lens and focussed on a pyro-electric detector. The distance Δz between the two laser foci can be adjusted with a (relative) accuracy better than 5 μm

equivalent H atoms, each with spin 1/2, four different spin species can be distinguished (A, B_1, B_2, and B_3). Symmetry considerations concerning the overall wavefunction require that every rovibrational state can only be coupled to a specific spin species, depending on the values of K_{-1} and K_{+1}. The corresponding statistical weights have been worked out to be 7 and 3 for A and B_i ($i=1,2,3$) species, respectively [3]. For the ground vibrational state, levels with K_{-1} and K_{+1} both even are referred to the A species.

Main emphasis will here be placed on the modelling of those parameters most important for the interpretation and evaluation of experiments on relaxation phenomena occurring in a jet [4, 5]. The next section will focus on some important details of the experimental set up. In Sect. 2 the results are presented; they are briefly discussed in Sect. 3.

1. Experimental

The general features of our experimental apparatus have been described elsewhere [5, 6]. In short, it is a double resonance experiment on a free molecular jet using two narrow-band IR lasers, viz. a CO_2 waveguide laser and a Color Center Laser (CCL; linewidth $< \sim 2$ MHz). Since the jet configuration is of crucial importance to our experiment, it will be discussed in more detail here.

The use of a free molecular jet in a double resonance experiment permits one to probe the low temperature regime not attainable in bulk gas (due to condensation). A schematic drawing of the jet used in our experiments is given in Fig. 2. The jet itself is formed by expanding ethylene at a stagnation pressure P_0 [usually 53 kPa (400 Torr)] through a circular stainless steel nozzle ($d=0.50$ mm) at room temperature (296 K). The nozzle can be opened and closed by means of a pressurized-air driven piston (Martonair M/7010/15). Directly below the jet expansion chamber is a 1200 m^3/h rootspump (Edwards EH 1200) backed by a 180 m^3/h rotary pump (Leybold SV 180). This combination is able to maintain a background pressure of about 40 Pa (0.3 Torr) when 53 kPa of ethylene is expanded. The jet is crossed perpendicular to its symmetry axis (taken as z-axis) by the CO_2 waveguide laser (along the x-axis) and the CCL (Burleigh FCL-20; along the y-axis). Both lasers are focussed on the jet axis, with focal widths of about 80 μm and 70 μm for the CO_2 laser and CCL, respectively (e^{-2}-points), thus providing the spatial resolution required for local probing of jet properties. Taking the origin of our coordinate system in the sonic plane of the nozzle, we call the distance between this plane and the center of the foci of CO_2 laser and CCL $z_{E(xcitation)}$ and $z_{P(robing)}$, respectively.

Behind the jet, the CCL is focussed onto a pyroelectric detector. Measurements can be made in two ways. In both cases the pyro signal is lock-in detected (Ortec 9501E), with a reference signal derived from a mechanical, variable speed chopper. When measuring the absorption of the CCL beam by the jet (without

CO_2 laser), the chopper is used to modulate the CCL beam. The pyro signal is now directly proportional to the incident CCL intensity. To increase sensitivity, part of the beam is split off before the jet expansion chamber, chopped by the same chopper and detected by a PbS detector. The (stronger) latter signal is passed through a phase shifter and an attenuator and can be made exactly equal in phase and in magnitude to the pyro signal (without jet). The lock-in amplifier is then used to detect the difference signal. This set up has the advantage that the jet absorption signals can be measured against a nearly zero background signal.

If, on the other hand, we want to detect the changes in absorption of the CCL beam brought about by the presence of the CO_2 laser beam, the CCL is applied unmodulated and the chopper is used to modulate the CO_2 laser beam. In this case, the pyro signal is proportional to the changes in incident CCL intensity caused by the modulated CO_2 laser. The PbS detector is now used to monitor the CCL intensity before the jet. This detection scheme has been used in order to determine the local flow velocity in the jet. In these experiments, the CO_2 laser (a home-built CO_2 waveguide laser, max. output power ca. 5 W) was tuned to pump the $(4,1,3)\rightarrow v_7(5,0,5)$ transition on resonance ($10P(10)$ line of the $^{12}CO_2$ laser, 98 MHz detuned [1], which is within the scanning range of the waveguide laser). It was frequency stabilized using a Lansing lock-in stabilizer (model 80.215).

Two stepper motors enable the CO_2 laser focus and the nozzle to be shifted up and down separately with respect to the (fixed) CCL focus (that is: along the z-axis). This way we can vary the distance below the nozzle at which CCL and CO_2 laser beams cross the jet axis. An Apple IIe was used to control the two stepper motors. The output of the lock-in with which the pyro signal was detected could be sampled by the Apple via a 12-bit A/D-convertor. In the case of double resonance measurements, between 20 and 100 samples of the lock-in output (depending on the S/N-ratio) were taken, statistically averaged and stored on diskette. With a 10(60) s integration time, a fractional change in CCL absorption of $5\times10^{-5}(1\times10^{-5})$ was detectable. These lower limits appeared to be determined by the noise in CCL intensity.

Measurements of the absorption of the CCL beam by the jet (in order to characterize the jet properties, as described below) are taken using the difference signal method described above. The Apple is now used to alternately open and close the nozzle. In each case, 70 samples of the lock-in output (difference signal) are taken and averaged. The difference between signals with the nozzle open and closed corresponds to the jet absorption. Depending on the strength of the absorption, between 12 and 40 difference signals were averaged and stripped of clearly deviating points (3σ criterion).

The ethylene gas was supplied by Air Liquide and used without further purification [purity, as stated by the manufacturer, 99.9%; main impurities being other hydrocarbons (<800 ppm; water content <25 ppm)].

2. Results

Those jet parameters we are mainly interested in are the local temperature (rotational and parallel translational), number density and flow velocity. The rotational temperature T_{rot} and the number density ϱ can be determined by measuring the jet absorption of CCL radiation for a number of transitions starting from different rotational levels. We assume the parallel translational temperature T_{trans} to be equal to T_{rot}. The flow velocity can be measured using a double resonance technique, as proposed by Veeken [8].

2.1. Temperature and Density

Since absorption of (laser) radiation by gas molecules is determined by, among other things, temperature and density of that gas, both these parameters can in principle be obtained from absorption measurements. In the appendix a relation between the jet absorption and the local, on-axis temperature and number density in the jet is derived. The resulting expression for $A_{JK}\equiv[\ln(I_0/I)/H_{JK}g_{JK}]$ has the form [see Appendix, (A 7)]

$$A_{JK}=\text{const}\,\frac{z\varrho(z)}{Q(z)v_f(z)}\exp\left(-\frac{E_{JK}}{kT_{rot}(z)}\right) \tag{1}$$

and from this equation it is easily seen that a plot of $\ln A_{JK}$ as a function of E_{JK} for constant z (a so called Boltzmann plot) should yield a straight line (if, at least, a thermal equilibrium exists). The slope of this line yields $1/kT_{rot}(z)$, while from the intercept with the $E_{JK}=0$-axis the number density $\varrho(z)$ can be extracted. The accuracy with which $\varrho(z)$ can be determined depends directly on the accuracy with which the flow velocity $v_f(z)$ and the transition strength are known. These quantities affect $T_{rot}(z)$ only in a weaker sense.

It should be noted, that the absorption of CCL radiation as measured by the pyro-electric detector is due to the total absorption pathlength in the jet expansion chamber and therefore also contains a contribution from the background gas. Thanks to the increased pumping capacity as compared to earlier experiments [6, 7], this background contribution is only small (typically about 1–5% of the total absorption). Nevertheless, it is corrected for in the following way. The width of the jet can be determined by measuring the total absorption in the jet expansion chamber for different positions x_p of the CCL focus (see

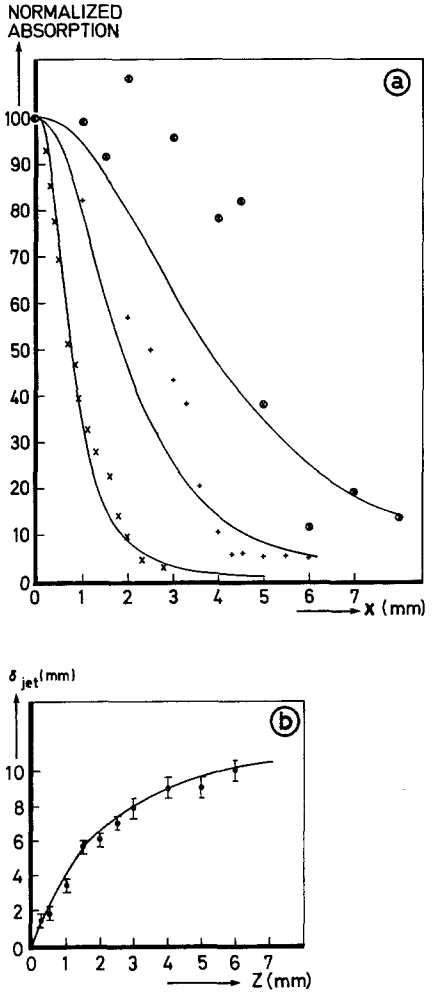

Fig. 3a, b. Determination of the jet width. The CCL probes the $^rR(4,0,4)$ transition in the ν_9 fundamental band (lower level at 18.2 cm^{-1}). **a** CCL absorption by the jet as a function of displacement along the x-axis for three different distances below the nozzle: 1.10 mm (×), 2.74 mm (+), and 5.50 mm (⊗). The solid curves represent model calculations taken from [20], with parameters adapted to our expansion conditions. **b** Full width of the jet as a function of distance below the nozzle. The solid curve is intended only to guide the eye

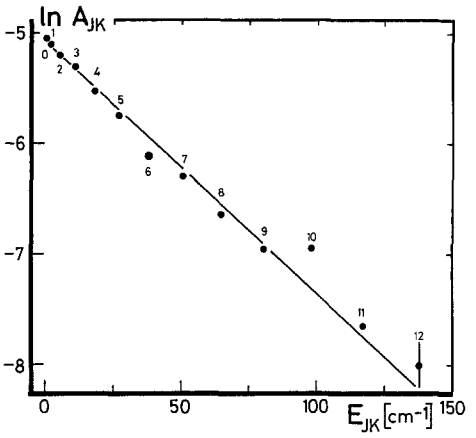

Fig. 4. Boltzmann plot. This plot represents the rotational population distribution in a 53 kPa (400 Torr) expansion of pure C_2H_4, 1.10 mm below the nozzle. The distribution is thermal, corresponding to a temperature of 63(3) K (solid line). The datapoints correspond to $^rR(J,0,J)$ transitions from the ν_9 band with $J=0$–12; A_{JK} is defined in the text. Error bars (one standard deviation) correspond to the point size for $J=0$ and increase to the size drawn for $J=12$. The ^rR (10, 0, 10) transition is overlapped by another transition (viz. the $^pR(11,0,11)$ [2])

Figs. 2 and 3). The CCL should be tuned to a low-J transition, for which the lower level is better populated in the jet than in the background gas. If x_p crosses the jet boundary, the contribution of the jet to the total absorption vanishes, which causes a more or less drastic decrease in the absorption signal (Fig. 3a). From this, a rather accurate measure of the jet width δ_{jet} for every z_P can be obtained (Fig. 3b). Since the total absorption pathlength is known (20 mm) and the background gas absorption over this pathlength can easily be measured, the contribution of the background gas absorption to the total absorption can be determined and afterwards subtracted. What is left is the contribution of the jet to the measured absorption and this can be used to construct Boltzmann plots, which in their turn yield $T_{rot}(z)$ and $\varrho(z)$. Care has been taken not to saturate any transition.

Within experimental error all Boltzmann plots correspond to a thermal rotational population distribution; an example is given in Fig. 4. These plots have been constructed using only absorption signals on ^rR transitions ($\Delta K_{-1}=\Delta J=1$) of the ν_9 band, starting from levels with $K_{-1}=0$. Local resonances tend to affect ν_9 line intensities but the $K_{-1}=0$ series is nearly unperturbed [9]. An additional advantage of using $K_{-1}=0$ levels is that they show no doubling, that is, there is only one K_{+1} component (viz. $K_{+1}=J$). The final results are plotted in Figs. 5 and 6. For determining T_{rot} we used the level energies as calculated by Fayt [9], although for calculating the rotational partition function $Q(z)$ the approximate formula for the energy levels of a slightly asymmetric top was used (see e.g. Townes and Schawlow [10]):

$$E(J,K_{-1},K_{+1})\approx\tfrac{1}{2}(B+C)J(J+1)+(A-\tfrac{1}{2}(B+C))w, \quad (2)$$

in which A, B, and C are the usual rotational constants (taken from Herlemont et al. [1]) and $w\approx K^2_{-1}$. Hönl-London factors H_{JK} are taken from Fayt [9]; they are calculated using asymmetric top wavefunctions for upper and lower states.

In Fig. 5 the rotational temperature on the jet axis is plotted as a function of the reduced distance below the nozzle. For large distances and especially for the

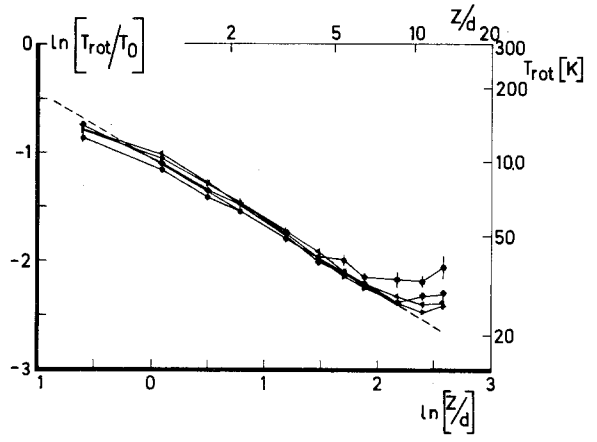

Fig. 5. On-axis rotational temperature in the jet as a function of distance below the nozzle for different stagnation pressures (13 kPa (100 Torr; ●), 27 kPa (200 Torr; ◆), 53 kPa (400 Torr; ▶) and 107 kPa (800 Torr; ◀)). The dashed curve represents a fit of the 400 Torr data to (3)

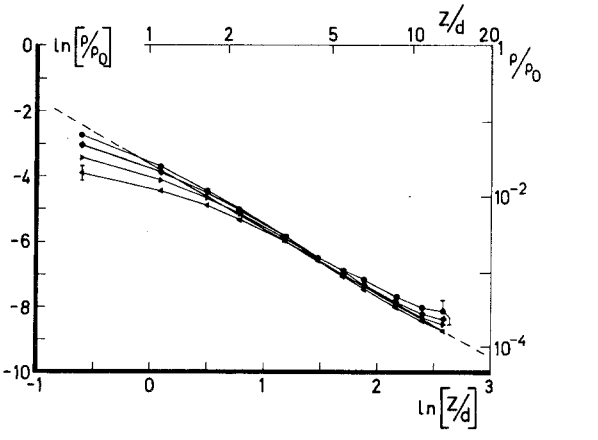

Fig. 6. On-axis number density in the jet as a function of distance below the nozzle for different stagnation pressures (13 kPa (100 Torr; ●), 27 kPa (200 Torr; ◆), 53 kPa (400 Torr; ▶) and 107 kPa (800 Torr; ◀)). The dashed curve represents a fit of the 400 Torr data to (4)

lower stagnation pressures, T_{rot} can be seen to freeze. For smaller distances the relation between T_{rot} and the distance z takes the form (e.g. [11])

$$\frac{T_{rot}(z)}{T_0} = K_T \left(\frac{z}{d}\right)^{-2(\gamma-1)}, \tag{3}$$

where T_0 is the stagnation temperature (296 K), d is the nozzle diameter (0.50 mm) and $\gamma = c_p/c_v$. A fit of our results against this model yields $K_T = 0.345(9)$[1] for a stagnation pressure of 53 kPa (400 Torr; it is only slightly different for the other pressures) and $\gamma = 1.31(3)$. This value of γ corresponds to the value expected for a jet expansion in which the vibrational degrees of freedom play no role in the cooling process. The fact that the curves for different stagnation pressures nearly coincide indicates the absence of excessive clustering. If clustering were present, the heat released in the formation of the complexes would increase the jet temperature. The temperature curves for higher stagnation pressures would then be situated significantly above those for lower pressures [6].

The results on the number density on the jet axis are plotted in Fig. 6. Here also, the curves for different stagnation pressures nearly coincide, which is another indication for the absence of significant cluster formation. The deviations observed for smaller distances from the nozzle reflect the influence of pressure broadening, which has not been taken into account in our derivation of (1). The smaller deviations for larger values of z/d are not significant in view of the increased uncertainty due to decreasing absorption signals. For a (2-dimensional) expansion from a circular nozzle, one expects the density to decrease with the square of the distance from the nozzle. If we fit our data to the following model [11]

$$\frac{\varrho(z)}{\varrho_0} = K_\varrho \left(\frac{z}{d}\right)^{-r}, \tag{4}$$

we find indeed $r = 1.97(5)$. For K_ϱ we find the value of 0.027(2) (400 Torr expansion).

2.2. Flow Velocity

In applying the double resonance technique to the measurement of relaxation times in a jet [4–6], the required time resolution is also determined by the flow velocity of the jet molecules. Usually, one assumes that all energy released during the rotational cooling in the expansion goes into the translational degrees of freedom. This leads to an expression for the flow velocity [12]

$$v_f(z) = v_\infty \left(1 - \frac{T_{rot}(z)}{T_0}\right)^{1/2}, \tag{5}$$

with $v_\infty = \sqrt{\frac{\gamma}{\gamma-1}\frac{2kT_0}{m}}$, the final flow velocity for an ideal expansion. Our experimental set up, with jet axis, pump laser and probe laser mutually perpendicular, lends itself naturally for an in situ measurement of the flow velocity. The idea is shown in Fig. 7a, in which the CO_2 laser is taken perpendicular to the plane of the paper. Not too close to the nozzle, the molecules in the jet propagate along (straight) streamlines. The position of the CO_2 focus on the y-axis, y_E, determines which of these streamlines are excited. The excited molecules can then be detected by the CCL. All molecules have a

[1] Errors represent one standard deviation in units of the last digit

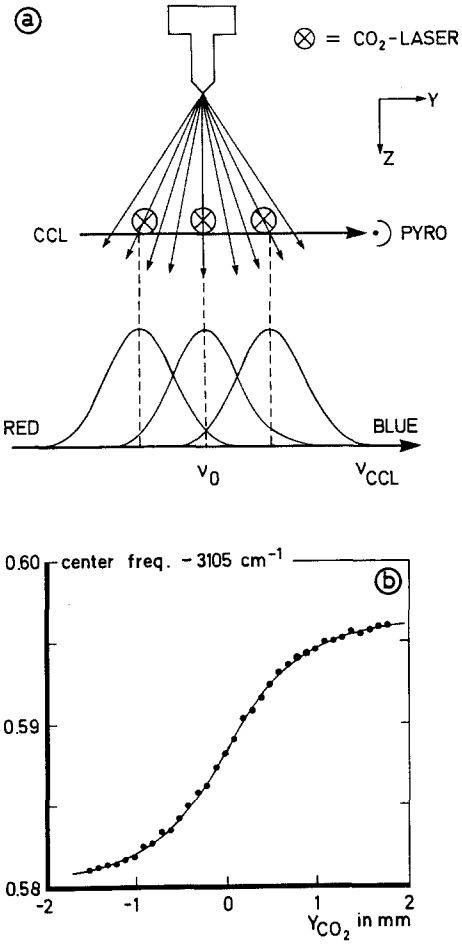

Fig. 7a, b. Determination of the flow velocity of the jet molecules. **a** Schematic view of the experimental set up. The CO_2 laser can be made to excite different streamlines of the jet. The center frequency of the IRIRDR signal is determined by the Doppler shifted molecular absorption frequency. **b** Center frequency of the IRIRDR signal as a function of position (along the CCL direction) of the pump laser focus. The solid line represents a fit to (6). The CCL is tuned to the $v_7(5,0,5) \rightarrow v_7 + v_9(5,1,4)$ transition [13] and thus probes the upper level of the pumped transition

velocity component $v_{||}$ parallel to the direction of the CCL beam, given by $v_{||} = v_f \sin\theta$, and their absorption frequencies therefore experience a Doppler-shift. The angle θ between a given streamline and the jet axis is determined by the position of the CO_2 focus, so that the Doppler-shifted absorption frequency can be written as

$$\nu_y = \nu_0 \left(1 + \frac{y_E}{(y_E^2 + z_E^2)^{1/2}} \frac{v_f}{c}\right) \tag{6}$$

where $(\nu_0)\nu_y$ is the (un)shifted absorption frequency.

Figure 7b shows the results for $z_E = z_P = 0.91$ mm. The solid curve is a fit of our datapoints to (6), assuming a constant flow velocity for all θ. If the resulting value is used in (5) to derive a value for v_∞, using the value of T_{rot} from the previous section, one finds $v_\infty = 944$ m/s, which is about 8% larger than would be expected from the theoretical value for an ideal expansion (being 871 m/s, for $\gamma = 1.3$). In the following, we use (5) to calculate flow velocities, but with v_∞ fixed on the experimentally derived value.

2.3. *Number of Collisions*

Nearly all of the cooling processes occurring in a jet are collision induced. The cooling of the parallel translational and the internal degrees of freedom as well as the relaxation of a perturbation in the equilibrium population distribution (introduced by e.g. a CO_2 laser, as in the previous section) are due to collisions between molecules and the rates at which these processes occur depend sensitively on the efficiency and the rate of intermolecular collisions. From this point of view, the distance z below the nozzle, the distance Δz travelled since the excitation or the corresponding elapsed time Δt are only of secondary importance.

It will be convenient to have a measure of the average number of collisions experienced by any molecule in the jet between the positions z_E and z_P. Since molecules themselves are not sharply delimited, a collision between two of them is an even more diffuse notion. For convenience, we will nevertheless consider the jet molecules as hard spheres, with an effective collision cross section σ_0 based on viscosity data [14]. Although some discussion is possible on the proper relationship between coefficient of viscosity and collision cross section, we will adopt the one used by other authors (Yuan and Flynn [15] and Häger et al. [16]) and use $\sigma_0 = 56.2$ Å^2.

The collision rates of molecules in different environments have been studied by Lubman et al. [17]. For the local gas kinetic binary collision rate in a jet, k_{jet}, they find:

$$k_{jet} = \sqrt{2}\varrho\sigma_0\bar{v}, \tag{7}$$

where the molecular velocity distribution (which should be considered as superimposed on the flow velocity v_f) is assumed to be Maxwellian, with an average (unidirectional) velocity $\bar{v} = \sqrt{8kT/\pi m}$. The number of gas kinetic collisions, N_C, between z_E and z_P can now be calculated in a straightforward way:

$$N_C(z_E, z_P) = \int_{t(z_E)}^{t(z_P)} k_{jet}\, dt. \tag{8}$$

Replacing the integration variable dt by dz/v_f and using our model functions of (3)–(5) for temperature, density and flow velocity, respectively, the final form of (8)

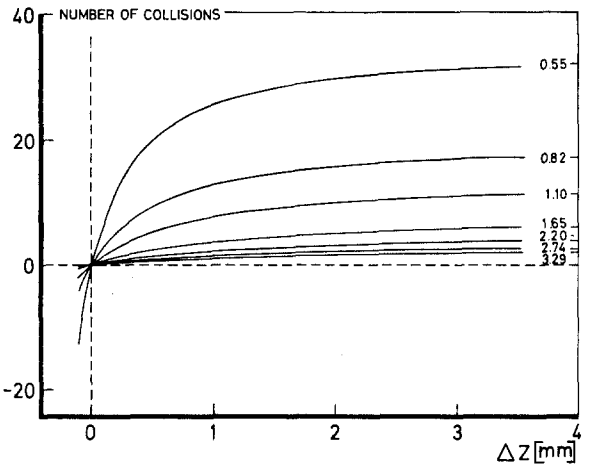

Fig. 8. The average number of gaskinetic collisions, calculated with $\sigma_0 = 56.2$ Å^2, as a function of distance Δz between pump and probe laser, for several distances of the pump laser below the nozzle (indicated at the right). A 400 Torr expansion is assumed, in which case the constant $N_C^{(0)}$ in (9) equals 88.7 mm^{-1}

becomes

$$N_C(z_E, z_P) = N_C^{(0)} \int_{z_E}^{z_P} \left(\frac{z}{d}\right)^{-(\gamma+1)} \times \left[1 - K_T \left(\frac{z}{d}\right)^{-2(\gamma-1)}\right]^{-1/2} dz \quad , \tag{9}$$

with $N_C^{(0)} = 4\sigma_0 K_\varrho \varrho_0 \left(\frac{K_T}{\pi} \frac{\gamma-1}{2\gamma}\right)^{1/2}$. Except for some special values of γ, the integration has to be carried out numerically. Fig. 8 illustrates the number of collisions as a function of $\Delta z = z_P - z_E$ for different values of z_E in the case of an expansion of 53 kPa (400 Torr) of ethylene. Obviously, the rarefaction and cooling of the gas in the jet cause a fast decrease in the number of collisions a molecule experiences in travelling some distance Δz. It should, however, be kept in mind that (9) and Fig. 8 deal only with the gas kinetic collision rate, calculated with a temperature independent cross section σ_0. This model is not necessarily representative for the inelastic collision processes which are responsible for relaxation phenomena.

3. Discussion

Free molecular jets have been the subject of much experimental and theoretical work, accounts of which have been given by Anderson [18] and numerous contributors to the proceedings of the Symposia on Rarefied Gas Dynamics [19]. In our choice of model functions we followed largely the account of Hagena [11], who also gives values corresponding to our K_T and K_ϱ of (3) and (4), for the two cases of $\gamma = 5/3$ and $\gamma = 7/5$. If we linearly extrapolate these data to our case of $\gamma = 1.31$ ($\approx 4/3$), this yields $K_T^{[111]} = 0.406$ and $K_\varrho^{[111]} = 0.0644$, both (and especially $K_\varrho^{[111]}$) larger than our results.

Two effects, however, have not been taken into account. First, the assumption of straight streamlines breaks down for distances very close to the nozzle (within a few nozzle diameters) and secondly, the viscosity of the gas causes a boundary layer to be formed along the nozzle wall, thereby reducing the effective nozzle diameter. Both features are discussed by Beyerinck and Verster [20]. Far away from the nozzle, the (straight) streamlines seem to originate from a point somewhat downstream of the sonic plane, due to the curvature of the streamlines close to the nozzle. When we use the data given in [20] on CO_2 expansions (CO_2 is expected to show about the same cooling behaviour as C_2H_4), the distance of this "virtual source point" below the nozzle can be calculated to be about 1 nozzle diameter, in our case. We, like Hagena [11], did not include this effect in our model functions, the main reason in our case being that they fitted experimental data better without correction for the virtual source.

The reduction of the effective nozzle diameter caused by the non-zero viscosity of the gas, can be calculated to be about 1% for our case and can therefore be neglected.

In all cases, our Boltzmann plots could well be fitted to a thermal rotational population distribution. As mentioned earlier, the occurrence of local resonances in the ν_9 band renders the transition strengths somewhat uncertain and this makes any slight curvature in a Boltzmann plot (Fig. 4) hard to interpret. Although in many cases the rotational population distribution in a jet cannot be described by a single temperature (see e.g. [21–23]), this phenomenon can be expected to be most important if the temperatures (which can always be defined with respect to any pair of levels) are comparable to or less than the energy level spacing. In our case, the lowest temperature reached being about 30 K, this criterion just starts to be met. Furthermore, in earlier experiments on a seeded molecular beam [24], the final temperature reached amounted to 7.7 K and the distribution (for $J \leqq 6$) still hardly showed any deviation from a thermal one. We therefore consider the effect of a possible a-thermal distribution (which may exist for energy levels above the uppermost one that we have included in our plots, the (12, 0, 12) level) not to be important in our experiments.

At larger distances below the nozzle ($z/d > \approx 7$) and lower stagnation pressures, the rotational temperature (Fig. 5) is larger than expected from (3). Two possible causes for this are the increasing contribution from the

barrel shock wave to the total absorption and/or rotational freezing. Although the importance of the barrel shock absorption certainly will increase with increasing z, the behaviour of the temperature curves as a function of stagnation pressure rather points to freezing. This onset of rotational freezing can, at least in principle, be used to obtain an estimate for the local rotational relaxation rates. Work along these lines is mostly due to Fenn and coworkers (see e.g. [25] and references in there). Assuming final rotational temperatures of 35 K (100 Torr expansion) and 29 K (200 Torr), we find values for the collision number for rotational relaxation between 5 and 8, which is about ten times larger than the collision number found in our experiments specifically aimed at obtaining these rates [4, 5]. It should be noted, that the present results depend very sensitively on the values adopted for the final temperatures and for γ. The agreement with our other experiments [4, 5] is, therefore, considered to be quite reasonable.

An interesting aspect of the double resonance method of Sect. 2.2 is that it allows the flow velocity to be determined locally. Since we detect the effect of the pump laser on one of the pumped levels, we do not depend on any relaxation and heating of the jet by the pump laser plays no role yet. Since we apply both pump and probe lasers relatively close to the nozzle, care must be taken to correct for a systematic error which may arise from the continuing expansion of the jet. When $\Delta z = z_P - z_E = 0$, that is, when pump and probe lasers overlap, molecules in a certain volume of the expansion, determined among other things by the width of the probe laser focus, are probed. If we increase Δz, this "initial volume" expands, while the size of the probe laser focus remains unchanged. Therefore, even if no relaxation would occur at all, the double resonance signal would be seen to decrease with increasing Δz, simply because an increasing part of the "initial volume" moves outside the region which is probed.

Even though it is not of importance in our experiments on the flow velocity, this geometrical artefact can easily be corrected for. When the jet expansion is considered separately in the directions parallel and perpendicular to the probe laser beam, it is seen that only the expansion perpendicular to the probe laser beam yields a significant contribution to the geometrical correction. The breadth of the "initial volume" perpendicular to the probe laser beam is determined by the width of the probe laser focus. After excitation at $z = z_E$, this breadth is increased by a factor z_P/z_E (with respect to its initial value) at the probing distance z_P. By multiplying the double resonance signals with the same factor this "dilution" can be corrected for. Parallel to the CCL beam, the size of the "initial volume" is determined by the Doppler shift of the molecular absorption frequency and the band width of the probe laser. Since the maximum Doppler shift of molecules at the edge of the pump laser focus amounts to about 3 MHz (cf. Fig. 7a), we expect to probe the whole focal width of the pump beam. Although the physical size of this region also increases with Δz, the initial Doppler shift changes only by about 10–15%, at most (due only to the increasing flow velocity). This is not enough to remove initially excited molecules out of the laser bandwidth (long term; estimated to be about 5 MHz) and, therefore, a correction is irrelevant. Finally, the "initial volume" also expands in the z direction due to the finite width of the flow velocity distribution. Since this spreading tends to broaden relaxation features rather than to remove molecules out of the probed region, it also is not to be included in the geometrical correction.

4. Conclusion

We have described a free molecular jet of ethylene and the experimental set up used to characterize its properties. The rotational population distribution of the jet appeared to be thermal for all distances below the nozzle studied (0.5–13.2 nozzle diameters). Values for the rotational temperature and number density in the jet have been determined from linear absorption measurements and were shown to be in reasonable agreement with literature data. From the onset of freezing of the rotational temperature in the case of relatively low pressure jet expansions, a (gas kinetic) collision number $N_{rot} \approx 6$ for the rotational relaxation was deduced (at $T_{rot} \approx 30$ K). A double resonance technique enabled the flow velocity to be measured locally, yielding a slightly larger value than expected for an ideal expansion. In applying such a double resonance technique in a jet, the jet expansion perpendicular to the probe laser gives rise to a systematic error in the double resonance signal strength. A simple geometrical argument shows that this error can easily be corrected for.

The number of gaskinetic collisions experienced by any molecule in travelling some distance along the jet axis has been calculated from the experimental data on local temperature, number density and flow velocity. In the range of distances below the nozzle studied, this number of collisions changes by about three orders of magnitude.

Appendix

For the absorption of weak, narrow-band, monochromatic (laser) radiation by some medium, one finds (see e.g. [26])

$$dI(v, y) = -\alpha(v, y)\varrho'(v, y)I(v, y)dy \qquad \text{(A1)}$$

in which $\alpha(v, y)$ is the local absorption coefficient, $\varrho'(v, y)$ is the local number density of absorbing molecules, and $I(v, y)$ is the local laser intensity.

The absorption coefficient $\alpha(v, y)$ can be expressed in terms of the Einstein coefficient for linear absorption, B_{01},

$$\alpha(v, y) = \frac{B_{01}}{2\pi\eta(v, y)c} h\nu F(v, y) \quad , \tag{A2}$$

in which $\eta(v, y)$ is the refractive index and $F(v, y)$ is the (normalized) transition line shape function.

B_{01} is related to the transition dipole moment $e|D_{01}|$ through

$$B_{01} = \frac{4\pi^3 e^2 |D_{01}|^2}{3\varepsilon_0 h^2}, \tag{A3}$$

where the requisite orientation average has already been carried out. Notice, by the way, that although the laser bandwidth is small compared to the absorption lineshape, the latter is much broader than the natural linewidth of a transition ($\sim 10^2$ Hz in our case) and therefore it is still allowed to use the Einstein coefficient approach.

The transition dipole moment $e|D_{01}|$ is conventionally written as $|\mu_{01}| \cdot H_{JK}^{1/2}$, where H_{JK} is the Hönl-London factor for the transition. For the ν_9 band of C_2H_4 we have $|\mu_{01}| = 0.0519(3)$ D [27]. Finally, ϱ' can be written as $f_{JK}\varrho$, in which ϱ is the total number density and f_{JK} the fraction of molecules in the lower level of the transition. Substituting all this into (A1), one finds

$$dI(v, y) = -\frac{2\pi^2 |\mu_{01}|^2 \nu}{3\varepsilon_0 h\eta(v, y)c} F(v, y) H_{JK} f_{JK} \varrho(y) dy \tag{A4}$$

and this has to be integrated over the absorption path through the jet.

Neglecting other broadening mechanisms, each position y corresponds to a specific Doppler shifted absorption frequency. If the laser frequency is tuned to the line center ν_0 (without Doppler shift), only a region around the jet axis contributes to the absorption. In this case, we can replace dy by $\frac{c}{v_f} z \frac{dv}{\nu}$. Furthermore, it is reasonable to assume that all other parameters do not change very much in the region where the lineshape function $F(v, y)$ is not close to zero. The integration is then easily carried out, yielding

$$I = I_0 \exp\left[-\frac{2\pi^2 |\mu_{01}|^2}{3\varepsilon_0 h\eta} \cdot \frac{z\varrho(z)}{v_f(z)} \cdot H_{JK} f_{JK}(z)\right]. \tag{A5}$$

The first factor in the exponential is a constant, C_{01}, in our measurements (equal to $3.35 \times 10^{-17}\,\mathrm{s^{-1}\,m^3}$). All other factors depend on z and/or the transition used. The fraction of molecules in the lower level of the transition can be written as

$$f_{JK} = \frac{g_{JK} \exp\left(-\frac{E_{JK}}{kT_{rot}(z)}\right)}{Q(z)}, \tag{A6}$$

where g_{JK} is the degeneracy of the lower level, E_{JK} is its energy and $Q(z)$ is the rotational partition function.

With the help of (A6), we can cast (A5) into an equivalent form,

$$A_{JK}(z) \equiv \frac{\ln(I_0/I)}{H_{JK} g_{JK}} = C_{01} \frac{z\varrho(z)}{Q(z) v_f(z)} \exp\left(-\frac{E_{JK}}{kT_{rot}(z)}\right) \tag{A7}$$

and this form is used throughout.

References

1. F. Herlemont, M. Lyszyk, J. Lemaire, Ch. Lambeau, M. de Vleeschouwer, A. Fayt: J. Mol. Spectr. **94**, 309 (1982)
2. A.S. Pine: Tunable Laser Survey of Molecular Air Pollutants, Final Report, NSF/ASRA/DAR 78-24562, MIT, Lexington, Mass., 1980
3. G. Herzberg: *Molecular Spectra and Molecular Structure*, Vol. II (van Nostrand Reinhold, New York 1945)
4. N. Dam, S. Stolte, J. Reuss: To be published
5. N. Dam: Thesis, Catholic University of Nijmegen, 1988
6. K. Veeken, N. Dam, J. Reuss: Chem. Phys. **100**, 171 (1985)
7. K. Veeken, J. Reuss: Z. Phys. D **1**, 113 (1986)
8. K. Veeken: Thesis, Catholic University of Nijmegen, 1985
9. A. Fayt: Private communication
10. C.H. Townes, A.L. Schawlow: *Microwave Spectroscopy* (Dover, New York 1975)
11. O.F. Hagena: Surf. Sci. **106**, 101 (1981)
12. G.M. McClelland, K.L. Saenger, J.J. Valentini, D.R. Herschbach: J. Phys. Chem. **83**, 947 (1979)
13. N. Dam, R. Engeln, J. Reuss, A. Fayt: To be published
14. R.C. Weast (ed.): *Handbook of Chemistry and Physics*, 59th ed. (CRC Press, West Palm Beach 1978)
15. R.C.L. Yuan, G.W. Flynn: J. Chem. Phys. **58**, 649 (1973)
16. J. Häger, W. Krieger, T. Rüegg, H. Walther: J. Chem. Phys. **70**, 2859 (1979)
17. D.M. Lubman, C.T. Rettner, R.N. Zare: J. Chem. Phys. **86**, 1129 (1982)
18. J.B. Anderson: "Molecular Beams from Nozzle Sources", In *Molecular Beams and Low Density Gas Dynamics*, ed. by P.P. Wegener (Dekker, New York 1974)
19. The often used empirical model of Ashkenas and Sherman can be found in Proc. 4th RGD Vol. II, ed. by J.H. de Leeuw (Academic, New York 1966) p. 84
20. H.C.W. Beyerinck, N.F. Verster: Physica **111**C, 327 (1981)
21. P. Wallraff, K.M.T. Yamada, G. Winnewisser: J. Mol. Spectrosc. **126**, 78 (1987)
22. P. Wallraff, K.M.T. Yamada, G. Winnewisser: Z. Naturforsch. **42**a, 246 (1987)
23. H. Zacharias, M.M.T. Loy, P.A. Roland, A.S. Sudbo: J. Chem. Phys. **81**, 3148 (1987)
24. N. Dam, C. Liedenbaum, S. Stolte, J. Reuss: Chem. Phys. Lett. **136**, 73 (1987)
25. C.G.M. Quah, J.B. Fenn, D.R. Miller: Proc. 11th RGD, Cannes, July 3–8, 1978, pp. 885–898
26. R. Loudon: *The Quantum Theory of Light*, 2nd edn. (Clarendon Press, Oxford 1983)
27. M. Dang-Nhu, A.S. Pine, A. Fayt, M. de Vleeschouwer, C. Lambeau: Can. J. Phys. **61**, 514 (1983)